Monoterpenes are the largest source of summertime organic aerosol in the southeastern United States

Haofei Zhang[a,b,1], Lindsay D. Yee[a], Ben H. Lee[c], Michael P. Curtis[d], David R. Worton[a,e,2], Gabriel Isaacman-VanWertz[a,3], John H. Offenberg[f], Michael Lewandowski[f], Tadeusz E. Kleindienst[f], Melinda R. Beaver[f], Amara L. Holder[g], William A. Lonneman[f], Kenneth S. Docherty[h], Mohammed Jaoui[f], Havala O. T. Pye[f], Weiwei Hu[i,j], Douglas A. Day[i,j], Pedro Campuzano-Jost[i,j], Jose L. Jimenez[i,j], Hongyu Guo[k], Rodney J. Weber[k], Joost de Gouw[j,l], Abigail R. Koss[j,l], Eric S. Edgerton[m], William Brune[n], Claudia Mohr[c,4], Felipe D. Lopez-Hilfiker[c,5], Anna Lutz[o], Nathan M. Kreisberg[e], Steve R. Spielman[e], Susanne V. Hering[e], Kevin R. Wilson[p], Joel A. Thornton[c], and Allen H. Goldstein[a,q,1]

[a]Department of Environmental Science, Policy, and Management, University of California, Berkeley, CA 94720; [b]Department of Chemistry, University of California, Riverside, CA 92521; [c]Department of Atmospheric Sciences, University of Washington, Seattle, WA 98195; [d]Department of Earth and Planetary Science, University of California, Berkeley, CA 94720; [e]Aerosol Dynamics Inc., Berkeley, CA 94710; [f]National Exposure Research Laboratory, Office of Research and Development, US Environmental Protection Agency, Research Triangle Park, NC 27711; [g]National Risk Management Laboratory, Office of Research and Development, US Environmental Protection, Agency, Research Triangle Park, NC 27711; [h]Jacobs Technology, Inc., Research Triangle Park, NC 27711; [i]Department of Chemistry and Biochemistry, University of Colorado Boulder, Boulder, CO 80309; [j]Cooperative Institute for Research in Environmental Sciences, University of Colorado Boulder, Boulder, CO 80309; [k]School of Earth and Atmospheric Sciences, Georgia Institute of Technology, Atlanta, GA 30332; [l]National Oceanic and Atmospheric Administration Earth System Research Laboratory, Boulder, CO 80305; [m]Atmospheric Research and Analysis, Cary, NC 27513; [n]Department of Meteorology, Pennsylvania State University, University Park, PA 16802; [o]Department of Chemistry and Molecular Biology, University of Gothenberg, SE-41296 Gothenberg, Sweden; [p]Chemical Sciences Division, Lawrence Berkeley National Laboratory, Berkeley, CA 94720; and [q]Department of Civil and Environmental Engineering, University of California, Berkeley, CA 94720

Edited by Mark H. Thiemens, University of California, San Diego, La Jolla, CA, and approved January 9, 2018 (received for review October 5, 2017)

The chemical complexity of atmospheric organic aerosol (OA) has caused substantial uncertainties in understanding its origins and environmental impacts. Here, we provide constraints on OA origins through compositional characterization with molecular-level details. Our results suggest that secondary OA (SOA) from monoterpene oxidation accounts for approximately half of summertime fine OA in Centreville, AL, a forested area in the southeastern United States influenced by anthropogenic pollution. We find that different chemical processes involving nitrogen oxides, during days and nights, play a central role in determining the mass of monoterpene SOA produced. These findings elucidate the strong anthropogenic–biogenic interaction affecting ambient aerosol in the southeastern United States and point out the importance of reducing anthropogenic emissions, especially under a changing climate, where biogenic emissions will likely keep increasing.

aerosol source apportionment | biogenic volatile organic compound oxidation | nitrogen oxides

Atmospheric aerosol is a highly variable and complex mixture largely composed of organic species derived from anthropogenic and biogenic emissions (1–3). Deciphering the composition, origins, and formation mechanisms of organic aerosol (OA) is crucial to unraveling its impacts on climate and human health (4, 5). The southeastern United States (US) represents an anthropogenic-influenced region with high biogenic volatile organic compound (BVOC) emissions (isoprene, C_5H_8; monoterpenes, $C_{10}H_{16}$; and sesquiterpenes, $C_{15}H_{24}$) in summertime, similar to numerous locations around the world. OA mass in the southeastern US correlates with anthropogenic tracers, while radiocarbon (^{14}C) measurements have consistently shown that OA is primarily modern (i.e., nonfossil) carbon that must be derived from BVOC oxidation, primary biological materials, biomass burning, or cooking (6, 7). This has led to uncertainty about OA origins and how its formation through oxidation processes (i.e., "secondary") is related to human activities (6, 8).

In past decades, the most widely used approaches for source apportionment of atmospheric OA rely either on a limited number of molecular markers (9, 10) or using bulk OA measurements coupled to factor analysis (2, 11). The first approach estimates contributions from specific sources assuming that the measured molecular markers have the same gas/particle partitioning and production yields from precursors in the atmosphere and in laboratory studies and are conserved in the atmosphere. These assumptions, however, are unreliable using common laboratory systems (e.g., refs. 12–14). Moreover, the parameters determining production yields could vary largely and it is unclear how to turn yields from laboratory studies into meaningful ambient yields. As a result, this approach is highly uncertain for determining source contributions to atmospheric OA. The second

Significance

Atmospheric fine organic aerosol impacts air quality, climate, and human health. Speciating and quantifying the sources of organic aerosol on the molecular level improves understanding of their formation chemistry and hence the resulting impacts. Such study, however, has not been possible due to the chemical complexity of atmospheric organic aerosol. Here, we provide comprehensive molecular characterization of atmospheric organic aerosol samples from the southeastern United States by combining state-of-the-art high-resolution mass spectrometry techniques. We find that monoterpene secondary organic aerosol accounts for approximately half of total fine organic aerosol. More importantly, the monoterpene secondary organic aerosol mass increases with enhanced nitrogen oxide processing, indicating anthropogenic influence on biogenic secondary organic aerosol formation.

Author contributions: H.Z., L.D.Y., and A.H.G. designed research; H.Z., L.D.Y., B.H.L., D.R.W., G.I.-V., J.H.O., M.L., T.E.K., M.R.B., A.L.H., W.A.L., K.S.D., M.J., H.O.T.P., W.H., D.A.D., P.C.-J., J.L.J., H.G., R.J.W., J.d.G., A.R.K., E.S.E., W.B., C.M., F.D.L.-H., A.L., N.M.K., K.R.W., J.A.T., and A.H.G. performed research; N.M.K., S.R.S., and S.V.H. contributed new reagents/analytic tools; H.Z., L.D.Y., B.H.L., M.P.C., J.H.O., W.H., H.G., J.d.G., J.A.T., and A.H.G. analyzed data; and H.Z. and A.H.G. wrote the paper.

The authors declare no conflict of interest.

This article is a PNAS Direct Submission.

[1]To whom correspondence may be addressed. Email: haofei.zhang@ucr.edu or ahg@berkeley.edu.

[2]Present address: National Physical Laboratory, Teddington, Middlesex TW11 0LW, United Kingdom.

[3]Present address: Department of Civil and Environmental Engineering, Virginia Polytechnic Institute and State University, Blacksburg, VA 24061.

[4]Present address: Department of Environmental Science and Analytical Chemistry, Stockholm University, SE-106 91 Stockholm, Sweden.

[5]Present address: Tofwerk AG, CH-3600 Thun, Switzerland.

This article contains supporting information online at www.pnas.org/lookup/suppl/doi:10.1073/pnas.1717513115/-/DCSupplemental.

approach, in particular, coupling high-time-resolution aerosol mass spectrometry (AMS) that measures bulk aerosol chemical composition to positive matrix factorization (PMF) has proven successful in resolving OA from a limited number of specific sources (e.g., some portion of OA from isoprene oxidation and biomass burning) (15–17). However, this approach loses specificity for OA from many other important sources (such as monoterpene oxidation) due to lack of unique signatures that are identifiable by AMS. Often, the largest fraction of the OA mass in AMS–PMF analyses is operationally defined by levels of oxidation and not assigned to specific sources.

During the summertime Southern Oxidant and Aerosol Study (SOAS) campaign in the southeastern US, the AMS–PMF-resolved isoprene secondary OA (SOA) combined with biomass burning OA together account for about 30% of total fine OA mass (16, 17). Additional analyses have apportioned another 5–12% of fine OA mass to particle-phase organic nitrates (pONs) associated with nitrate radical (NO_3) oxidation of BVOC during nighttime (18, 19). To be consistent with ^{14}C measurements requires inferring that a large fraction of the remaining unsourced OA (on the order of ~50% of total OA mass) also has nonfossil origins, but direct evidence of such a source has been missing. Xu et al. (19) suggested that NO_3 oxidation of monoterpenes is likely responsible for a large fraction of nighttime OA mass based on AMS–PMF results correlating with pONs, but definitive source identification with direct tracers remains lacking. Molecular-level comprehensive characterization of the OA is not only vital for unambiguous source identification but also informative for mechanistic understanding of SOA formation chemistry. Particularly, elucidating and quantifying the molecular composition of SOA provides the key to explaining the correlations of SOA with anthropogenic tracers and the long-term observations of reductions in anthropogenic emissions correlating to decreasing OA mass in this region for the past 15 y (20, 21). Here, we address these questions and provide quantitative results regarding previously unresolved OA sources with a focus on monoterpene SOA (MTSOA) and its relation to anthropogenic emissions in the southeastern US.

Results and Discussions

We comprehensively characterized OA composition with molecular-level details by performing complementary analyses of OA collected in Centreville, AL, during summer 2013, as part of the SOAS field campaign (16, 17). Continuous 4-h fine particulate matter (PM_1) samples were collected throughout the field campaign and analyzed off-line by thermal desorption and derivatization with 2D gas chromatography (GC×GC) coupled to a high-resolution time-of-flight mass spectrometer (HTOF-MS) with dual ionization. Electron impact (EI) ionization is used for mass spectral matching to libraries, and vacuum UV (VUV) photoionization is used to retain molecular-weight ions for chemical formula identification (13, 22). Thus, largely improved molecular separation and identification are obtained, leading to over 800 individual species being measured (Fig. 1*A*), all of which were then quantified using authentic standards, surrogate standards, or by extrapolating peak response factors based on standards with similar chemical structures and GC retention times. See *Detailed Experimental Procedure* for a detailed description.

On-line characterization of particle-phase OA chemical composition was performed by an HTOF chemical ionization mass spectrometer (CIMS) with a filter inlet for gases and aerosols (FIGAERO) using iodide-adduct (I^-) ionization (23). The average mass spectrum measured by FIGAERO-HTOF-CIMS (hereafter, CIMS) during SOAS is shown in Fig. 1*B*. Major OA components in this data have been identified as SOA produced predominantly through BVOC oxidation, including pONs (18, 19) and multifunctional acids and hydroperoxides (24). I^--CIMS has high sensitivity to these compounds (23), while GC×GC-HTOF-MS (hereafter, GC×GC) does not but is better at detecting less polar species, hence measurements from these two instruments complement each other. Additional measurements made during SOAS and utilized in our analyses include AMS

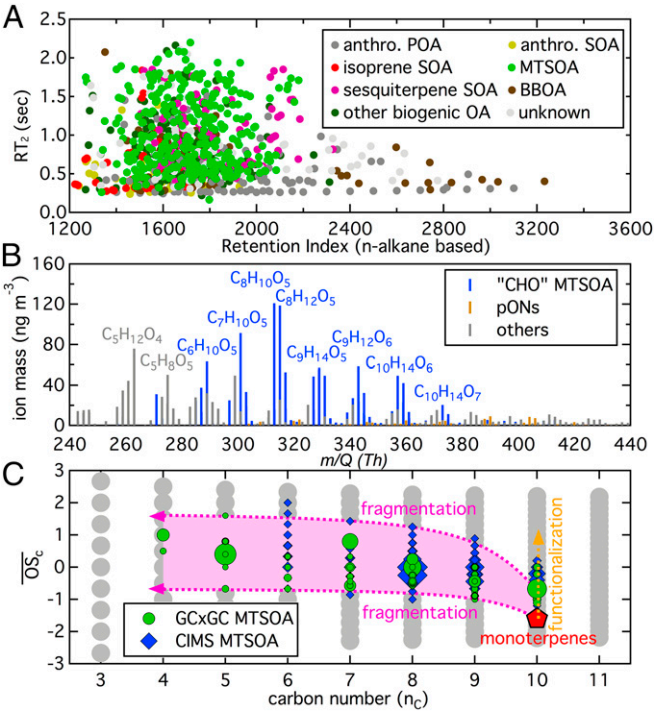

Fig. 1. OA molecular-level measurements. (*A*) Organic species measured by GC×GC with *x* axis first dimension retention in *n*-alkane based index and *y* axis second dimension retention in time (RT_2). Symbols represent individual organic species, with color indicating assigned source-based group ("anthro." is short for "anthropogenic" and "BBOA" for "biomass burning OA"). Symbol size is uniform for clear illustration. (*B*) Representative mass spectrum measured by CIMS using I^- ionization. The *m/Q (Th)* in blue are assigned to non-nitrogen-containing MTSOA. The chemical formulae of the main peaks (I^- removed) are labeled with the mass spectrum. (*C*) All speciated MTSOA by GC×GC (green) and CIMS (blue), in the $\overline{OS}_c$–n_C space. Gray represents all possible organic formulae. Generic pathways from monoterpenes (red pentagon) to functionalization and fragmentation products are shown. Size of MTSOA symbols indicate their average mass during SOAS.

PM_1 OA, water-soluble organic carbon (WSOC), and fossil vs. modern carbon in OA by ^{14}C measurements.

To interpret results from the field measurements, laboratory ozonolysis experiments of α-pinene, limonene, and myrcene that represent the dominant monoterpene species present in ambient air during SOAS were conducted in a flowtube reactor (13). The SOA samples were collected and analyzed by GC×GC using the same method as for the ambient OA samples. Injecting monoterpenes in excess of O_3 allowed simultaneous hydroxyl radical (OH) oxidation of monoterpenes to occur because OH is a product from monoterpene ozonolysis. The purpose of these experiments was to generate a relatively large "library" of MTSOA species but which does not include all likely MTSOA species for the ambient samples. Known MTSOA tracers from ozonolysis and OH oxidation such as pinonic acid ($C_{10}H_{16}O_3$) and pinic acid ($C_9H_{14}O_4$) were observed in the laboratory experiments, along with hundreds of previously unreported compounds. A number of previously reported MTSOA tracers observed in the presence of nitrogen oxides ($NO_x \equiv NO + NO_2$) [e.g., 3-hydroxyglutaric acid ($C_5H_8O_5$) (25), 3-acetylpentanedioic acid ($C_7H_{10}O_5$) (10), 2-hydroxy-4,4-dimethylglytaric acid ($C_7H_{12}O_5$) (10), and 3-methyl-1,2,3-butanetricarboxylic acid (MBTCA, $C_8H_{12}O_6$) (25), etc.] were not found in our experiments but were included in the MTSOA library for ambient sample analysis. In the SOAS OA samples 89 matched species were identified as from monoterpene oxidation. Linear regression analysis of the remaining field data species' time series with those of the 89 species was performed: compounds with correlation to any known MTSOA

species of correlation coefficient (r^2) >0.60 were assigned to MTSOA. Organic species known to originate from isoprene oxidation, biomass burning, or anthropogenic emissions all had correlation r^2 <0.40 with the known MTSOA species. Thus, this threshold minimizes incorrect assignments (probability ~0.1%). Another 245 species were assigned to MTSOA, for a total 334 MTSOA species. Laboratory chamber studies of α-pinene oxidation were also conducted with CIMS measurements. A number of non-nitrogen-containing C_6–C_{10} species were observed in both the field measurements and chamber studies, supporting their relation to monoterpene oxidation. The possibility that these CIMS-measured compounds assigned to MTSOA overlap with chemicals derived from other sources [e.g., levoglucosan, $C_6H_{10}O_5$, from biomass burning, or sesquiterpene oxidation, or accretion products from isoprene oxidation (26)] cannot be ruled out. However, these chemicals are unlikely to interfere strongly with C_6–C_{10} MTSOA during SOAS due to their relatively low abundances. Chemical formulae with 5 or fewer and 11 or more carbons measured by CIMS that appeared in both field and α-pinene chamber experiments were not considered as MTSOA as they are not distinguishable from possible isoprene or other oxidation products in ambient samples.

A carbon oxidation state ($\overline{OS}_C$)–carbon number (n_C) space (27) is used to describe the chemical identities, properties, and transformation capacities of the MTSOA species captured by the two instruments (Fig. 1*C*). The C_{10} species containing oxygen must be formed by only adding functional groups to the C_{10} monoterpene backbone (i.e., functionalization) and the C_4–C_9 species must be formed by C–C bond scission (i.e., fragmentation) together with functionalization (27). CIMS observed more species with higher $\overline{OS}_C$, many of which are likely multifunctional hydroperoxides. By comparing the mass and time series of identical chemicals between the two measurements, overlapped MTSOA species are determined (see *Detailed Experimental Procedure*) and are discussed later in this paper. In addition to MTSOA, each of the other species measured by GC×GC was assigned to one of the following source-specific groups: anthropogenic primary OA (POA), anthropogenic SOA, biomass burning OA, isoprene SOA, sesquiterpene SOA, and other biogenic OA. These assignments were based on either known chemical identities by mass spectra or good correlations with the identified chemicals. Among these groups, sesquiterpene SOA has been less characterized. To sufficiently assign sesquiterpene SOA species we analyzed archived SOA samples from oxidation experiments of six sesquiterpenes under various conditions by GC×GC (28, 29). Hence, 69 sesquiterpene SOA species were assigned using the same approach as the MTSOA assignments. Fewer than 10% of compounds do not correlate with any characterized species and were grouped as "unknown." Thus, we characterized and quantified all of the observed compounds (Dataset S1) measured by GC×GC and assigned most of them into source-based groups.

Comprehensive time series of all characterized OA components are stacked (excluding the overlapped MTSOA mass) and shown in Fig. 2*A*, in comparison with AMS PM_1 OA. For the OA sampling periods when measurements from AMS, GC×GC, and CIMS were all available averaged contributions of identified sources to total AMS PM_1 OA based on the combined data were calculated (all data averaged to filter sampling time resolution). As shown in Fig. 2*B*, the source-based groups measured by GC×GC together account for 39% of the total OA mass, over half of which are MTSOA. The "other biogenic OA" group primarily consists of compounds that individually correlate modestly (r^2 of 0.4–0.6) with identified BVOC-derived SOA species and poorly with those in anthropogenic POA, anthropogenic SOA, or biomass burning OA. This group as a whole correlates strongly with MTSOA ($r^2 = 0.83$, $n = 254$), indicating that monoterpene oxidation is likely the main origin of this group, in which case total MTSOA measured by GC×GC contributes 23% to total OA. MTSOA measured by CIMS contributes at least 26% to total OA. The overlapped MTSOA species between the two instruments represent ~3% of the total OA. Excluding the overlapped species, MTSOA from the combined datasets accounts for 42% (± 4%) of total OA mass (+ 4% if the "other biogenic OA" are all considered as MTSOA; – 4% if the GC×GC-determined MTSOA without chemical formula

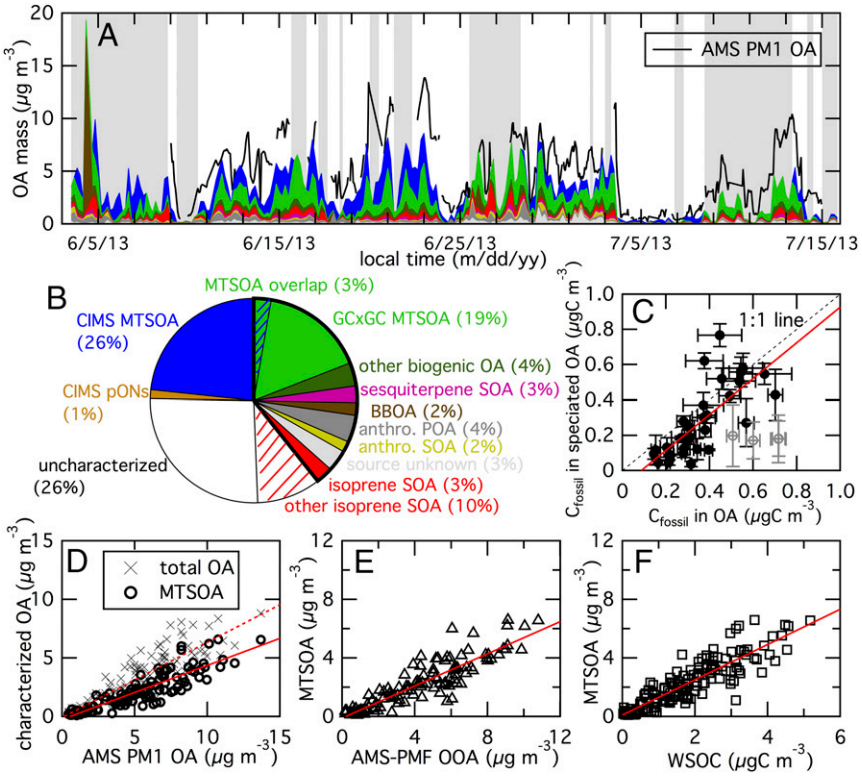

Fig. 2. Comprehensive OA speciation results. (*A*) Time series of summed speciated OA compared with AMS PM_1 OA. Periods when either AMS or CIMS was not sampling are shaded gray. (*B*) Pie chart representing contributions from speciated OA groups to total AMS PM_1 OA (during periods with all datasets available). (*C*) Comparison of C_{fossil} mass (1σ) speciated in this work with that measured by ^{14}C ($r^2 = 0.54$). Good agreement (except for 06/19–06/22, shown in gray symbols) suggests the sum of speciated anthropogenic POA and SOA accounts for most C_{fossil} mass and the remaining OA are dominated by modern carbon. (*D*) Correlations of total characterized OA (×, $r^2 = 0.77$, slope = 0.64) and MTSOA (○, $r^2 = 0.80$, slope = 0.46) with AMS PM_1 OA. (*E*) Correlation of total characterized MTSOA with AMS–PMF OOA ($r^2 = 0.81$, slope = 0.55). (*F*) Correlation of total characterized MTSOA with WSOC ($r^2 = 0.78$).

identification are all overlapped by CIMS measurements). The second-largest source contributor to total OA mass is isoprene oxidation. Although the isoprene SOA tracers measured by GC×GC only account for 3% of total OA, AMS–PMF results suggest a 13% contribution from isoprene SOA (during the selected periods, the two measurements correlate at $r^2 = 0.72$, $n = 190$). This difference is consistent with previous CIMS observations (30, 31) suggesting ~80% of isoprene SOA species such as organosulfates and oligomers were not detected by GC×GC. Thus, another 10% of OA mass is apportioned to isoprene SOA. Overall, the characterized OA together explains ~74% of total OA mass. The uncertainties in the reported source contributions are mainly from surrogate standard use (for GC×GC) and ionization sensitivity estimates (for CIMS). Overall, the uncertainties in GC×GC and CIMS are ~40% (*Detailed Experimental Procedure*) and 50% (18), respectively.

OA in the southeastern US is primarily modern carbon (6). Measurements of ^{14}C from daily high-volume filters ($PM_{2.5}$) during SOAS give an average modern carbon fraction of 0.83 ± 0.05. We estimated speciated fossil carbon (C_{fossil}) mass based on anthropogenic POA and SOA mass measured by GC×GC and compare with ^{14}C-measured C_{fossil} in OA (Fig. 2*C*). This comparison demonstrates that most of C_{fossil} is quantitatively accounted for by characterized anthropogenic POA and SOA. Thus, it indirectly confirms that most OA is composed of modern carbon, which is mainly from monoterpene oxidation followed by isoprene and sesquiterpene oxidation and the relatively minor contribution from biomass burning. As shown in Fig. 2*D*, the total characterized OA ($r^2 = 0.77$, $n = 113$) and MTSOA ($r^2 = 0.80$, $n = 113$) both correlate strongly with total PM_1 OA mass measured by AMS. Remarkably, we observed a strong correlation ($r^2 = 0.81$, $n = 118$) between MTSOA and the total oxygenated OA (OOA) AMS–PMF factor (1, 2) with a slope of 0.55 (Fig. 2*E*), suggesting that 55% of the OOA are accounted for as characterized MTSOA. This finding sheds light on a long-debated question about the specific sources of AMS–PMF-resolved OOA factors, at least in BVOC-dominated regions. Prior work has used WSOC as a surrogate for total ambient SOA (6). Here we find that MTSOA is also strongly correlated with WSOC ($r^2 = 0.78$, $n = 151$) (Fig. 2*F*). These correlations for MTSOA are significantly higher than those for all of the other groups (Table S1). Note that MTSOA does not correlate with isoprene SOA, ruling out the possibility that our assigned MTSOA species are accretion products of isoprene. The strong correlations of OOA and WSOC only with MTSOA imply that the comprehensive characterization and source-oriented grouping provide unprecedented insights toward reconciling molecular and bulk composition measurements of atmospheric OA, clearly supporting the conclusion that MTSOA accounts for a dominant fraction of OA during SOAS. The similarity in the environmental conditions (20, 21), gas and particle tracers (Table S2), monoterpenes/isoprene ratios (Fig. S1), and bulk OA composition (16, 19) between the Centreville site and many other locations in the southeastern US suggests the results from SOAS are representative of the southeastern US during summertime.

Although individual MTSOA species present strong and different diurnal cycles reflecting their unique formation chemistry (examples shown in Fig. S2), total MTSOA mass had a relatively "flat" diurnal pattern during the SOAS field campaign, with the average at ~3 $\mu g \cdot m^{-3}$ for the month of June (Fig. 3*A*). The Community Multiscale Air Quality model (CMAQ, v5.1) that is widely used to simulate and predict regional air pollutants and to guide environmental regulations significantly underpredicts observed MTSOA mass and fails to capture its diurnal pattern (32). This discrepancy could be largely due to the fact that the parameterization used in CMAQ relies on laboratory studies that do not adequately simulate atmospheric processes, such as autoxidation of monoterpene peroxy radicals (RO_2), which is known to produce low-volatility products that readily form MTSOA (24). This process, although occurring only for a small fraction of monoterpene RO_2 (24), could substantially impact total MTSOA mass due to its high SOA formation potential. As shown in Fig. 3*B*, RO_2 bimolecular lifetimes (determined by reactions with NO, HO_2, and RO_2) are on the order of ~10 s and 200 s during daytime and nighttime, respectively, similar to autoxidation timescales (24, 33), supporting the likely relevance of autoxidation. Current regional models of total OA may be improved if they can reasonably implement the chemical processes related to MTSOA formation.

In this work we identify monoterpenes as the major OA source in the summertime southeastern US from a molecular-level and measurement-based perspective. No assumptions regarding production yields of SOA from monoterpene oxidation allows a more accurate and quantitative understanding of MTSOA mass, which is also key to assessing the importance of anthropogenic–biogenic interactions for OA production. In principle, MTSOA formation is directly determined by (*i*) rates of initial RO_2 production (or other intermediate products) from monoterpene oxidation and (*ii*) effectiveness of converting RO_2 into MTSOA through multiple pathways. The average diurnal profiles of monoterpene oxidation, RO_2 formation, and the subsequent bimolecular RO_2 fates are estimated based on real-time measurements (except for total RO_2 concentrations, which are modeled by CMAQ) and known rates (Fig. 4 *A* and *B*). Many of these chemical processes are impacted by NO_x, which can be anthropogenic but can also be emitted by soil microbes as a function of temperature (34). For example, in a NO_x-limited environment such as the southeastern US atmospheric processes involving NO_x directly enhance the oxidants important for monoterpene oxidation: OH (35), O_3 (36, 37), and NO_3 (38). Total MTSOA are averaged to the filter sample time resolution for periods with both GC×GC and CIMS measurements available, excluding precipitation events. Since MTSOA formation chemistry pathways are very different during daytime and nighttime, data are separated further to examine MTSOA formation mechanisms at different times. Based on a combination of the sunlit time and the timing of boundary layer height changes (Fig. S3), the 4-h data from 1200–1600 hours and 1600–2000 hours are analyzed as daytime samples and those from 2000–0000 hours and 0000–0400 hours as nighttime samples.

Daily NO_x peaks in the morning during the SOAS field campaign and reacts with various inorganic and organic chemicals, from which SOA can be produced. Hence, we examine daytime MTSOA as a function of total processed NO_x (i.e., NO_z, the sum of NO_3, HNO_3, HONO, alkyl nitrates, peroxynitrates, and pONs). A strong correlation is observed between MTSOA and NO_z ($r^2 = 0.82$, $n = 19$) (Fig. 4*C*), suggesting that daytime MTSOA is highly related to NO_x processing. The enhancement of MTSOA with NO_z is likely due to the combined influences of

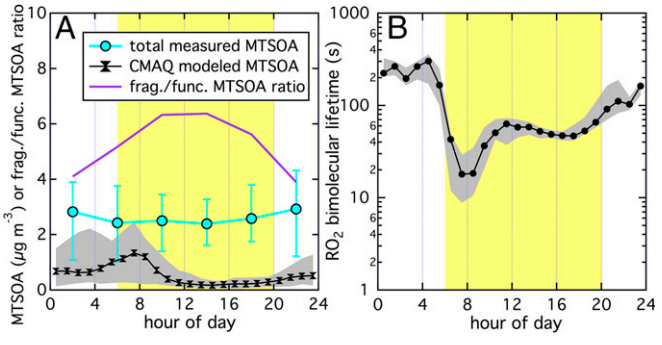

Fig. 3. Diurnal profiles of MTSOA mass and RO_2 bimolecular lifetime. (*A*) Average MTSOA mass (1σ) by local time of day, compared with CMAQ model, both for the month of June. The ratio of fragmentation MTSOA (C_4–C_9) to functionalization MTSOA (C_{10}) (frag./func. MTSOA ratio) shows an increase in fragmentation products during daytime. (*B*) RO_2 bimolecular lifetime as a function of local time of day. Yellow represents sunlit times and gray represents interquartile of data.

elevated oxidants and increased RO_2 + NO chemistry. The first effect is evident based on the observation that MTSOA species at all n_C increase with daytime NO_z enhancement. Even though functionalized MTSOA (C_{10}) also increases with NO_z, the fraction of C_{10} MTSOA species in total MTSOA has a strong anticorrelation with NO_z ($r^2 = 0.68$, $n = 19$) (Fig. 4*C*). Combining this observation with the effect that the ratio of MTSOA from fragmentation chemistry (C_4–C_9 products) to functionalization chemistry (C_{10} products) is enhanced during daytime (Fig. 3*A*) clearly suggests that fragmentation products from the RO_2 + NO chemistry lead to the majority of daytime MTSOA. These findings are somewhat unexpected because RO_2 + NO reactions are typically considered less prominent in forming SOA as fragmentation products are generally more volatile (39). However, considering that RO_2 autoxidation efficiently adds oxygen to the molecules, creating multifunctional RO_2 (24, 33), production of fragmentation products followed by multifunctional RO_2 + NO can readily form low-volatility molecules.

During nighttime at SOAS prior studies have highlighted the importance of monoterpene oxidation by NO_3, which is primarily formed by NO_2 + O_3 (16, 19, 32, 40). Since ozonolysis is still the primary loss pathway of monoterpenes at night (~80% on average; see Fig. 4*A*), the direct quantitative influence of NO_3 oxidation on MTSOA remains uncertain. Eighty-eight pONs species measured by CIMS were reported to contribute ~1–3% of total OA mass (Fig. 2*B*), 30 of which were associated with monoterpene NO_3 oxidation (18). Unspeciated total nighttime pONs are estimated to account for 5–12% of total OA mass (19). Neither result explains a large portion of the observed nighttime MTSOA. Nighttime MTSOA normalized by total monoterpene concentration was found to exhibit good correlation ($r^2 = 0.69$, $n = 13$) with the fraction of monoterpene oxidation by NO_3 (f_{MT+NO3}) over various nights (Fig. 4*D*) but is independent of O_3 concentrations. This trend is in excellent agreement with that of the sum of CIMS-speciated monoterpene-derived pONs, showing that our observed total MTSOA species, although not containing nitrogen, increase with f_{MT+NO3}. The non-nitrogen-containing MTSOA might be formed from NO_3 oxidation followed by pONs hydrolysis. However, non-nitrogen-containing fractions in MTSOA from these mechanisms reported by laboratory studies (~40%) (41, 42) and the CMAQ modeling results (~75%, assuming fast hydrolysis and products being nonvolatile) (32) are much lower than our nighttime observations (>95%). This difference suggests a large portion of the observed nighttime MTSOA must be from ozonolysis or another unrecognized process, although the reason for its enhancement with f_{MT+NO3} remains elusive.

Historical data from summertime Centreville, AL show that significant decreases in NO_x levels have occurred in the past 15 y, with associated decreases of OA, consistent with the trend in the relationship between MTSOA and oxidized NO_x reported here (20). Projected NO_x decreases in the future will likely lead to further decreases in MTSOA and hence total OA. However, as global climate changes increases in soil NO_x and BVOC emissions (43) could make regional particulate matter control more challenging in the southeastern US despite effective anthropogenic NO_x emission reductions. On the global scale, significant fractions of ambient OA are composed of modern (e.g., refs. 44 and 45) and oxidized OA (2), beyond that which can be explained by isoprene SOA and biomass burning OA. Based on our results we suggest that MTSOA may account for much of the unexplained modern OA in regions with significant monoterpene emissions, and hence quantifying how reducing pollutant emissions can mediate MTSOA is critical for designing regulations to control total OA.

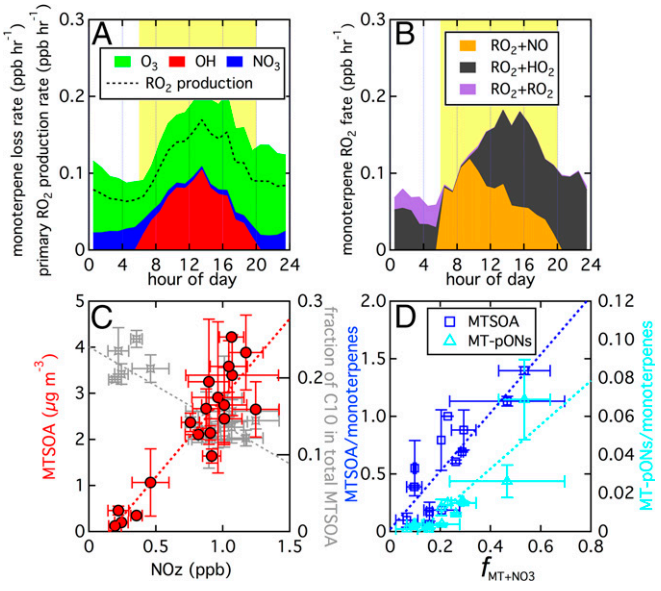

Fig. 4. NO_x influence on MTSOA formation. (*A*) Diurnal pattern of monoterpene loss by O_3, OH, and NO_3 oxidation. Black dashed line represents total primary RO_2 production rate, assuming 60% RO_2 yield from monoterpene ozonolysis. (*B*) Diurnal pattern of monoterpene bimolecular RO_2 loss. In *A* and *B*, OH oxidation and RO_2 + NO pathway are forced to be zero at night, regardless of measurements. (*C*) Correlation of daytime (1200–2000 hours) MTSOA with NO_z (1σ). (*D*) Correlations of nighttime (2000–0400 hours) MTSOA (left *y* axis, 1σ) and total monoterpene-produced pONs (MT-pONs, right *y* axis, 1σ) normalized by monoterpenes with f_{MT+NO3}. All correlations are statistically significant ($P < 0.005$).

Materials and Methods

Collection of Fine Aerosol Samples During SOAS. During the SOAS field campaign 254 submicron aerosol samples were collected on quartz filters (prebaked at 600 °C for 12 h to remove organics) using a sequential sampler at ~120 L·min^{-1} every 4 h from June 3 to July 15, 2013. All filters were stored in baked foil at −20 °C before analysis.

Laboratory Terpene Oxidation Experiments. We conducted monoterpene (including α-pinene, limonene, and myrcene) ozonolysis experiments in a flow tube reactor at University of California, Berkeley to identify measurable MTSOA tracers. SOA was collected for 20 min–10 h on Quartz fiber filters (47-mm Tissuquartz, prebaked at 600 °C; Pall Life Science) after passing through a charcoal denuder (8-inch, 480-channel; MAST Carbon). In addition, α-pinene ozonolysis chamber experiments were conducted at University of Washington with on-line measurements by CIMS. Filter samples from prior US EPA sesquiterpene oxidation experiments (28, 29), including β-caryophellene, α-humulene, α-cedrene, β-farnesene, α-copaene, and aromadendrene (irradiation in the presence of NO_x and ozonolysis), were also analyzed by GC×GC. Initial conditions and other details of laboratory experiments are provided in *Detailed Experimental Procedure*.

GC×GC Measurements. Collected filter samples (two to five punches, 0.8–2.0 cm^2) were thermally desorbed (in helium) at a steady ramp to 320 °C into a gas chromatograph (GC, Agilent 7890) using a thermal desorption system (TDS3; Gerstel) with in-situ gas-phase derivatization by *N*-methyl-*N*-trimethylsilyl trifluoroacetamide (Sigma-Aldrich), which converts all polar hydroxyl groups into trimethylsilyl ester groups so that the molecules can get through the nonpolar GC columns. Thermal desorption of aerosol samples from filters can result in some decomposition of accretion products or oligomeric material, but the resulting fragments as measured by GC×GC still serve as useful OA source tracers (17, 30, 31). The slow temperature ramp and the on-line derivatization should help minimize additional thermal decomposition of labile molecules. Analytes were separated by 2D GC and detected using HTOF-MS. The first dimension column separates species primarily by volatility and the second dimension column separates species primarily by polarity. Traditional 70-eV EI ionization was used for all samples. Selective samples were also analyzed using 10.5-eV VUV photons, which is a soft photoionization that causes minimal fragmentation and enhances detectable parent molecular-weight ions so that chemical formulae (for most species) can be resolved (46, 47). The VUV analysis was conducted at the Advanced Light Source, Lawrence Berkeley National Laboratory. Details of GC×GC data analysis are provided in *Detailed Experimental Procedure*.

CIMS Measurements. On-line analysis of particle-phase composition using a FIGAERO coupled to CIMS was deployed at SOAS. Detailed description of this measurement can be found in previous studies (18, 23, 30). For this work, CIMS measurements using iodide as reagent ions determine that the oxidized chemical formulae with C_6–C_{10} range and suitable H and O numbers (one degree of double bond equivalence is allowed) are MTSOA (96 species). All these assigned MTSOA chemical formulae are consistent with laboratory-generated α-pinene ozonolysis SOA. A list of chemical formulae measured by CIMS assigned to MTSOA is shown in Table S3. Previously identified pONs species related to monoterpene NO_3 oxidation (used in Fig. 4*D*) are also listed in Table S3.

ACKNOWLEDGMENTS. We thank Prof. Ronald Cohen's group at University of California, Berkeley for useful discussion. This work was supported by NSF Grants AGS-1250569 and AGS-1644406. W.H., D.A.D., and J.L.J. were supported by NSF Grant AGS-1360834 and US Department of Energy (DOE) (BER/ASR) Grant DE-SC0016559. The VUV measurements performed at the Advanced Light Source, Lawrence Berkeley National Laboratory were supported by the director, Office of Energy Research, Office of Basic Energy Science, of the DOE under Contract DE-AC02-05CH11231. The US EPA through its Office of Research and Development partially funded and collaborated in the research described here. The manuscript was subjected to peer review and has been cleared for publication. Mention of trade names or commercial products does not constitute endorsement or recommendation for use.

1. Zhang Q, et al. (2007) Ubiquity and dominance of oxygenated species in organic aerosols in anthropogenically-influenced Northern Hemisphere midlatitudes. *Geophys Res Lett* 34:L13801.
2. Jimenez JL, et al. (2009) Evolution of organic aerosols in the atmosphere. *Science* 326: 1525–1529.
3. Goldstein AH, Galbally IE (2007) Known and unknown organic constituents in the Earth's atmosphere. *Environ Sci Technol* 41:1514–1521.
4. Goldstein AH, Koven CD, Heald CL, Fung IY (2009) Biogenic carbon and anthropogenic pollutants combine to form a cooling haze over the southeastern United States. *Proc Natl Acad Sci USA* 106:8835–8840.
5. Seagrave J, et al. (2006) Lung toxicity of ambient particulate matter from southeastern U.S. Sites with different contributing sources: Relationships between composition and effects. *Environ Health Perspect* 114:1387–1393.
6. Weber RJ, et al. (2007) A study of secondary organic aerosol formation in the anthropogenic-influenced southeastern United States. *J Geophys Res Atmos* 112: D13302.
7. Geron C (2011) Carbonaceous aerosol characteristics over a Pinus taeda plantation: Results from the CELTIC experiment. *Atmos Environ* 45:794–801.
8. Carlton AG, Pinder RW, Bhave PV, Pouliot GA (2010) To what extent can biogenic SOA be controlled? *Environ Sci Technol* 44:3376–3380.
9. Schauer JJ, et al. (1996) Source apportionment of airborne particulate matter using organic compounds as tracers. *Atmos Environ* 30:3837–3855.
10. Kleindienst TE, et al. (2007) Estimates of the contributions of biogenic and anthropogenic hydrocarbons to secondary organic aerosol at a southeastern US location. *Atmos Environ* 41:8288–8300.
11. Ulbrich IM, Canagaratna MR, Zhang Q, Worsnop DR, Jimenez JL (2009) Interpretation of organic components from positive matrix factorization of aerosol mass spectrometric data. *Atmos Chem Phys* 9:2891–2918.
12. Rudich Y, Donahue NM, Mentel TF (2007) Aging of organic aerosol: Bridging the gap between laboratory and field studies. *Annu Rev Phys Chem* 58:321–352.
13. Zhang H, et al. (2015) Fundamental time scales governing organic aerosol multiphase partitioning and oxidative aging. *Environ Sci Technol* 49:9768–9777.
14. Kessler SH, et al. (2010) Chemical sinks of organic aerosol: Kinetics and products of the heterogeneous oxidation of erythritol and levoglucosan. *Environ Sci Technol* 44: 7005–7010.
15. Budisulistiorini SH, et al. (2013) Real-time continuous characterization of secondary organic aerosol derived from isoprene epoxydiols in downtown Atlanta, Georgia, using the Aerodyne Aerosol Chemical Speciation Monitor. *Environ Sci Technol* 47: 5686–5694.
16. Xu L, et al. (2015) Effects of anthropogenic emissions on aerosol formation from isoprene and monoterpenes in the southeastern United States. *Proc Natl Acad Sci USA* 112:37–42.
17. Hu WW, et al. (2015) Characterization of a real-time tracer for isoprene epoxydiols-derived secondary organic aerosol (IEPOX-SOA) from aerosol mass spectrometer measurements. *Atmos Chem Phys* 15:11807–11833.
18. Lee BH, et al. (2016) Highly functionalized organic nitrates in the southeast United States: Contribution to secondary organic aerosol and reactive nitrogen budgets. *Proc Natl Acad Sci USA* 113:1516–1521.
19. Xu L, Suresh S, Guo H, Weber RJ, Ng NL (2015) Aerosol characterization over the southeastern United States using high-resolution aerosol mass spectrometry: Spatial and seasonal variation of aerosol composition and sources with a focus on organic nitrates. *Atmos Chem Phys* 15:7307–7336.
20. Hidy GM, et al. (2014) Chemical climatology of the southeastern United States, 1999-2013. *Atmos Chem Phys* 14:11893–11914.
21. Blanchard CL, Hidy GM, Shaw S, Baumann K, Edgerton ES (2016) Effects of emission reductions on organic aerosol in the southeastern United States. *Atmos Chem Phys* 16:215–238.
22. Worton DR, et al. (2017) Improved molecular level identification of organic compounds using comprehensive two-dimensional chromatography, dual ionization energies and high resolution mass spectrometry. *Analyst (Lond)* 142:2395–2403.
23. Lopez-Hilfiker FD, et al. (2014) A novel method for online analysis of gas and particle composition: Description and evaluation of a filter inlet for gases and AEROsols (FIGAERO). *Atmos Meas Tech* 7:983–1001.
24. Ehn M, et al. (2014) A large source of low-volatility secondary organic aerosol. *Nature* 506:476–479.
25. Claeys M, et al. (2007) Hydroxydicarboxylic acids: Markers for secondary organic aerosol from the photooxidation of α-pinene. *Environ Sci Technol* 41:1628–1634.
26. D'Ambro EL, et al. (2017) Isomerization of second-generation isoprene peroxy radicals: Epoxide formation and implications for secondary organic aerosol yields. *Environ Sci Technol* 51:4978–4987.
27. Kroll JH, et al. (2011) Carbon oxidation state as a metric for describing the chemistry of atmospheric organic aerosol. *Nat Chem* 3:133–139.
28. Jaoui M, Kleindienst TE, Docherty KS, Lewandowski M, Offenberg JH (2013) Secondary organic aerosol formation from the oxidation of a series of sesquiterpenes: α-cedrene, β-caryophyllene, α-humulene and α-farnesene with O3, OH and NO3 radicals. *Environ Chem* 10:178–193.
29. Offenberg JH, et al. (2017) Predicting thermal behavior of secondary organic aerosols. *Environ Sci Technol* 51:9911–9919.
30. Lopez-Hilfiker FD, et al. (2016) Molecular composition and volatility of organic aerosol in the Southeastern U.S.: Implications for IEPOX derived SOA. *Environ Sci Technol* 50:2200–2209.
31. Isaacman-VanWertz G, et al. (2016) Ambient gas-particle partitioning of tracers for biogenic oxidation. *Environ Sci Technol* 50:9952–9962.
32. Pye HOT, et al. (2015) Modeling the current and future roles of particulate organic nitrates in the Southeastern United States. *Environ Sci Technol* 49:14195–14203.
33. Crounse JD, Nielsen LB, Jørgensen S, Kjaergaard HG, Wennberg PO (2013) Autoxidation of organic compounds in the atmosphere. *J Phys Chem Lett* 4:3513–3520.
34. Travis KR, et al. (2016) Why do models overestimate surface ozone in the Southeast United States? *Atmos Chem Phys* 16:13561–13577.
35. Monks PS (2005) Gas-phase radical chemistry in the troposphere. *Chem Soc Rev* 34: 376–395.
36. Chameides WL, Lindsay RW, Richardson J, Kiang CS (1988) The role of biogenic hydrocarbons in urban photochemical smog: Atlanta as a case study. *Science* 241: 1473–1475.
37. Thornton JA, et al. (2002) Ozone production rates as a function of NO_x abundances and HO_x production rates in the Nashville urban plume. *J Geophys Res* 107:ACH 7-1–ACH 7-7.
38. Wayne RP, et al. (1991) The nitrate radical: Physics, chemistry, and the atmosphere. *Atmos Environ* 25:1–203.
39. Ng NL, et al. (2007) Effect of NOx level on secondary organic aerosol (SOA) formation from the photooxidation of terpenes. *Atmos Chem Phys* 7:5159–5174.
40. Ayres BR, et al. (2015) Organic nitrate aerosol formation via NO3 + biogenic volatile organic compounds in the southeastern United States. *Atmos Chem Phys* 15: 13377–13392.
41. Boyd CM, et al. (2015) Secondary organic aerosol formation from the β-pinene+ NO3 system: Effect of humidity and peroxy radical fate. *Atmos Chem Phys* 15: 7497–7522.
42. Fry JL, et al. (2014) Secondary organic aerosol formation and organic nitrate yield from NO3 oxidation of biogenic hydrocarbons. *Environ Sci Technol* 48:11944–11953.
43. Heald CL, et al. (2008) Predicted change in global secondary organic aerosol concentrations in response to future climate, emissions, and land use change. *J Geophys Res Atmos* 113:2156–2202.
44. Bench G, Fallon S, Schichtel B, Malm W, McDade C (2007) Relative contributions of fossil and contemporary carbon sources to PM 2.5 aerosols at nine Interagency Monitoring for Protection of Visual Environments (IMPROVE) network sites. *J Geophys Res Atmos* 112:D10205.
45. Gelencsér A, et al. (2007) Source apportionment of PM2.5 organic aerosol over Europe: Primary/secondary, natural/anthropogenic, and fossil/biogenic origin. *J Geophys Res Atmos* 112:D23S04.
46. Isaacman G, et al. (2012) Improved resolution of hydrocarbon structures and constitutional isomers in complex mixtures using gas chromatography-vacuum ultraviolet-mass spectrometry. *Anal Chem* 84:2335–2342.
47. Chan AWH, et al. (2013) Detailed chemical characterization of unresolved complex mixtures in atmospheric organics: Insights into emission sources, atmospheric processing, and secondary organic aerosol formation. *J Geophys Res Atmos* 118: 6783–6796.